Tokamak level performance in the optimized stellarator Wendelstein 7-X with stable peaked density profiles

S. Bannmann,[1,*] O. Ford,[1] S. A. Bozhenkov,[1] T. Stange,[1] R. Lopez-Cansino,[2] A. Langenberg,[1] M. Wappl,[1] J. Brunner,[1] G. Fuchert,[1] T. Gonda,[1] D. Hartmann,[1] J. Knauer,[1] H. Laqua,[1] P. McNeely,[1] N. Pablant,[3] E. Pasch,[1] P. Poloskei,[1] K. Rahbarnia,[1] N. Rust,[1] F. Warmer,[1] R. C. Wolf,[1] and the W7-X Team

[1]*Max-Planck-Institute for Plasma Physics, Greifswald, Germany*

[2]*Department of Atomic, Molecular and Nuclear Physics, University of Seville, Seville, Spain*

[3]*Princeton Plasma Physics Laboratory, Princeton, New Jersey 08540, USA*

(Received 14 November 2025; accepted 30 March 2026; published 1 July 2026; corrected 3 August 2026)

Progress towards achieving net gain from nuclear fusion is typically characterized by the triple product $nT\tau$. Although stellarators have several benefits for a reactor, such as the inherent steady-state capability and the lack of disruptions, the maximum achieved triple product has historically lagged behind that of tokamaks. In the large optimized stellarator Wendelstein 7-X, a triple product of $(1.10 \pm 0.15) \times 10^{20}$ m^{-3} keV s has recently been achieved and held stable for 1.9 s. This marks an important step in stellarator core plasma performance and puts it in line with *H*-mode performance in similar sized tokamaks. The progress in Wendelstein 7-X performance is due to the suppression of ion-temperature-gradient turbulence by strong density gradients. In the record case, these are maintained by a fine balance of the core particle transport and central fueling using neutral beam injection. The duration of the scenario was limited in time only by technical restrictions of the neutral beam injectors and control of the divertor heat loads. This paper presents the result in the context of the leading magnetic confinement devices along with details of the scenario.

DOI: 10.1103/q59k-8m26

I. INTRODUCTION

Fusion plasma performance is often characterized by a single parameter, the triple product ($nT\tau_E$), which combines plasma density, ion temperature, and energy confinement time into a single number and is connected to the fusion power gain [1]. It is one of the central figures of merit across fusion reactor concepts [2] and the highest triple products achieved in large tokamaks [3] are close to the break even value, where the fusion power output becomes equal to the input power required to maintain the plasma. stellarators are a competing line of magnetic confinement devices and offer several benefits for a fusion reactor, such as inherent steady state operation without the need to drive plasma current, operation at high plasma densities as there is no hard density limit [4,5], an absence of disruptions, and simpler plasma control due to a lower susceptibility to MHD instabilities [5]. However, due to the poorer confinement properties of three-dimensional configurations without optimization [2,6,7] stellarators are traditionally perceived inferior to tokamaks in terms of the triple product performance. The quasi-isodynamic stellarator Wendelstein 7-X (W7-X) [8–10] was designed to improve confinement with numerical optimization of the magnetic field. Neoclassical, i.e., collisional, heat, and particle, losses were successfully reduced [11,12], proving the plausibility of high-temperature operation in a reactor. Yet, this is not sufficient to match the tokamak *H*-mode performance in most electron-cyclotron-resonance heated (ECRH) plasmas of W7-X, where the ion-temperature-gradient (ITG) mode driven turbulence limits the core ion temperature to 1.6 keV. This limit, known as ion temperature clamping [13], is also observed in, e.g., ASDEX-Upgrade *L*-mode plasmas [14]. In W7-X, the clamping limit can be overcome via generation of peaked electron density profiles, which stabilize the ITG turbulence [15,16]. Trapped electron modes (TEMs), which are driven by density gradients, remain stable due to the beneficial magnetic field geometry of W7-X [17–19]. While the ITG stabilization is similar to tokamaks, the reduced TEM level is W7-X specific and together they allow for large density and temperature gradients with reduced transport at low collisionality. Experimentally, improved confinement phases were established after injections of a short series of hydrogen ice pellets [16,20–22] or with the help of the neutral beam injection (NBI) system [23–26], which takes advantage of a particle pinch [27] and a regime of reduced particle diffusion [28]. The ion-scale turbulence suppression in these experiments was consistently confirmed by fluctuation measurements [29,30] and was also observed in the impurity channel [31,32]. However, so far such improved phases remained transient or did not exploit the full density range. Recently, the effect has been further explored with mixed

*Contact author: sebastian.bannmann@ipp.mpg.de

Published by the American Physical Society under the terms of the Creative Commons Attribution 4.0 International license. Further distribution of this work must maintain attribution to the author(s) and the published article's title, journal citation, and DOI. Open access publication funded by Max Planck Society.

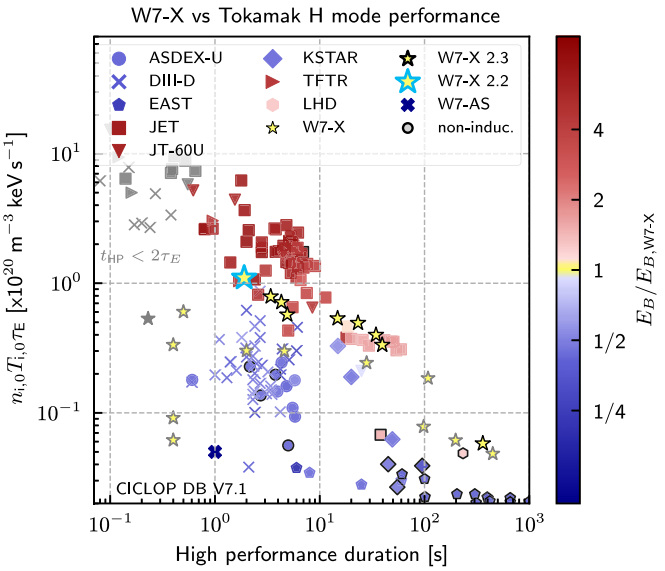


FIG. 1. Triple product computed from the central density and ion temperature plotted as a function of the duration of the high-performance phase. The achieved values in W7-X of the last campaigns are compared to tokamak *H*-mode plasmas (CICLOP DB 7.1 [38]). The presented record performance achieved in OP2.2 (discharge No. 20241204.072) is plotted as a cyan + yellow star. The color scale marks the ratio of the stored magnetic energy $E_B = VB_0^2/2\mu_0$ in the confined region to the W7-X value.

NBI and ECR heating (and pellet fueling [33]) and developed into a stable and reproducible operational scenario. The development culminated in plasma program No. 20241204.072, with a triple product value of $(1.10 \pm 0.15) \times 10^{20}$ m^{-3} keV s maintained for 1.9 s, limited only by the technical restrictions of the neutral beam injectors and control of the divertor heat loads. Stronger density and temperature gradients are maintained for a longer period than previously reported by selecting the optimum magnetic configuration and the specific combination of NBI and ECR heating to balance core fueling against increased particle diffusion present when adding ECRH. The result suggests that peaked density profiles can be used as a scenario for a stellarator reactor [34] to combine the benefits of a stellarator with the performance of the tokamak. With sufficient understanding of the particle transport, the reactor operational point could be self-consistently optimized for the required temperature gradient [35]. Such scaling up requires extensive gyrokinetic modeling including both heat and particle transport, which only recently became available for stellarators [36,37] and is yet to be validated against the empirical results presented here.

II. W7-X VERSUS TOKAMAK *H*-MODE PERFORMANCE

In Fig. 1 a comparison of the time-averaged triple product achieved in the high-performance (HP) phase of discharge No. 20241204.072 (labeled W7-X 2.2, cyan + yellow star; for the exact value, see Table I) to tokamak *H*-mode data are shown as a function of the duration. The tokamak data, taken from the database CICLOP DB V7.1 [38], cover a range of different *H*-mode operational regimes, including advanced scenarios such as negative central shear, noninductive current drive (fully noninductive tokamak data points are indicated by black marker edges in Fig. 1), and internal transport barriers (ITBs). Significant progress in terms of the plasma performance was made in W7-X in the last decade of operation, progressing from the earlier operational campaigns OP1 and OP2.1 (yellow stars with gray edges) to the last campaigns OP2.2 and OP2.3 (yellow stars with black and red edges). For reference, a relevant data point from the the preceding device Wendelstein 7-AS [39] is also plotted with a bold oblique cross. As a clear comparative measure between the Wendelstein and the tokamak data points the stored magnetic energy, computed as $E_B = VB_0^2/2\mu_0$, where V is the plasma volume and B_0 is the field on axis, is used. Not only does it approximately reflect the minor radius and magnetic field part of the gyro-Bohm scaling of the triple product [see Eq. (C9)] but it is also the main factor determining device cost. The ratio to the W7-X value of the stored magnetic energy is color coded in the figure. The new W7-X triple product value exceeds the quasistationary (lasting longer than $2\tau_E$) *H*-mode performance of tokamaks with less stored magnetic field energy than W7-X such as DIII-D, ASDEX-Upgrade, KSTAR, or EAST (blue in the color scale), and is on par with some discharges from JET or TFTR, devices with significantly more magnetic energy (red). In this sense, W7-X has achieved a competitive triple product given its size and magnetic field. A clear degradation of performance with the HP duration is seen in the tokamak data largely due to the almost linear scaling of confinement time with plasma current [40] which is inversely proportional to duration given a limited maximum voltage of the central solenoid. While noninductive current drive has been shown on several tokamaks (e.g., AUG [41], JET [42], DIII-D [43], EAST [44]), these typically achieve lower plasma currents and hence lower confinement. As confinement in optimized stellarators does not depend on plasma current, the HP duration of the W7-X points is restricted only by technical limits of systems that were not designed to be steady-state capable. In the last campaign (OP2.3) the discharge No. 20241204.072 was not repeated or extended as the kinetic plasma energy exceeded a safety limit imposed to avoid falsely triggering the quench detection system of the superconducting coils. This limit has now been removed and an extension in time up to 8 s, as set by NBI capabilities, will be possible in the next year. In the meantime, it was possible to extend this scenario with deliberately limited performance,

TABLE I. Energy confinement time and triple product in the high-performance phase of discharge No. 20241204.072.

Parameter	Value	Error	Unit	f_{ren}
$\overline{\tau_E}$	260	±15	ms	1.04
$\tau_E^{\max}$	286	±19	ms	1.14
$\tau_{E,\text{ISS04}}$	251	±12	ms	1.0
$\overline{n_{i,0}T_{i,0}\tau_E}$	1.10	±0.15	10^{20} m^{-3} keV s	
$n_{i,0}T_{i,0}\tau_E\vert^{\max}$	1.18	±0.17	10^{20} m^{-3} keV s	

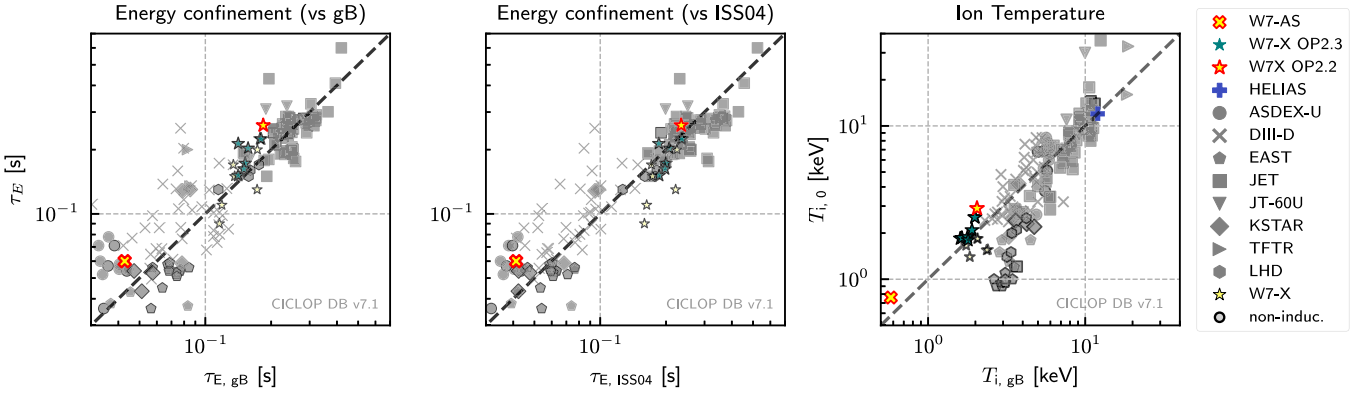


FIG. 2. W7-X high-performance discharges compared to tokamak *H*-mode data. Left: Achieved energy confinement time as s function of the value expected from tokamak fitted gyro-Bohm scaling. Tokamak data points where the high-performance phase was shorter than the reported energy confinement were excluded. Middle: Energy confinement time vs the ISS04 scaling [49]. The tokamak minor radii and ι values needed for the scaling expression were determined following Refs. [54,55] and $f_{\rm ren} = 1$ was used. Right: Experimentally achieved core ion temperature plotted as a function of the value expected from tokamak fitted gyro-Bohm scaling. The shown HELIAS point is a simple extrapolation of the presented gyro-Bohm scaling to stellarator reactor relevant machine parameters determined in other studies [56].

using a different magnetic configuration, achieving $n_i T_i \tau_E \sim 0.8 \times 10^{20}$ m^{-3} keV s for almost 4 s (see W7-X 2.3 points in Fig. 1), highlighting the steady state nature of the regime [33]. Finally, W7-X data points with a triple product of less than about 0.4×10^{20} m^{-3} keV s correspond to the baseline plasma operation without control of the density profile. Such plasmas have been extended already to hundreds of seconds [45], but lack the benefit of peaked densities in terms of performance. The peak triple product and confinement time achieved in discharge No. 20241204.072 are given in Table I along with their averages over the 1.9-s-long HP phase. The confinement time is computed from the measured diamagnetic energy W [46] and heating power $P_{\rm H}$ as $\tau_E = \frac{W}{P_{\rm H} - \dot{W}}$. The heating power includes the absorbed ECRH power and the injected neutral beam power reaching the plasma. The central ion density is computed from the measured electron density and the effective charge $Z_{\rm eff} = 1.5$ measured by visible Bremsstrahlung [47]. The dominant impurity species is carbon, as expected from the graphite plasma facing materials and confirmed by core carbon density measurements [48]. As a reference, the expected energy confinement from the intermachine ISS04 stellarator scaling [49] is given as well as the renormalization factor $f_{\rm ren} = \tau_E / \tau_{E,\rm ISS04}$. While the triple product is a convenient figure of merit, the same value can be obtained with linear changes in density, temperature, and confinement time that give significantly different fusion gain when far from the reaction optimum [2]. Particularly, stellarators do not have a hard density (Greenwald) limit [4,5] and hence can operate at very high densities. Therefore, an additional examination of the scaling of energy confinement time and plasma temperature is required.

III. ENERGY CONFINEMENT TIME SCALING

Previously, it was shown that both the tokamak *H* mode and the ISS04 energy confinement empirically scale gyro-Bohm-like in the normalized gyroradius ρ^* and scale only weakly with collisionality ν^* and β [50–52]. Combining the gyro-Bohm scaling $\tau_{E,\rm gB} \propto (\rho^*)^{-3}$ [53] with the experimental definition of τ_E gives the corresponding scalings of the confinement time $\tau_{E,\rm gB}$ and plasma temperature $T_{\rm gB}$ (more details in Ref. [52]):

$$T_{\rm gB} = c_1 \epsilon^{0.4} m^{-0.2} \left(\frac{P_{\rm H}}{n}\right)^{0.4} B^{0.8}, \tag{1}$$

$$\tau_{E,\rm gB} = c_2 a^3 \epsilon^{-0.6} m^{-0.2} \left(\frac{P_{\rm H}}{n}\right)^{-0.6} B^{0.8}. \tag{2}$$

Here, $\epsilon = \frac{a}{R}$ is the inverse aspect ratio, m the isotope mass, and c_1 and c_2 are constants determined from the data. The resulting scaling in τ_E is very similar to the one derived in Ref. [54] from a critical gradient tokamak heat transport model. While this simple approach facilitates the comparison between stellarators and tokamaks, it ignores effects of rotational transform, collisionality, and β on confinement. Despite this, it reproduces the general trends of the best confinement between machines well. This can be seen in Fig. 2, in which the achieved energy confinement times (left) and central ion temperatures (right) are plotted versus the gyro-Bohm values computed using Eqs. (1) and (2). For a consistent comparison between tokamak and stellarator data, the minor radius a in the gyro-Bohm scaling expressions was defined via the plasma volume [$a^2 = V/(2\pi^2 R)$] and accordingly the tokamak minor radii given in the database were adjusted as $a = a_{\rm tokamak}\sqrt{\kappa}$, where κ is the elongation factor (following Ref. [55]). The prefactors c_1 and c_2 have been fitted exclusively to the tokamak data in order to show how the stellarator results compare to a range of *H*-mode operational regimes. The HP discharges of W7-X reach a similar τ_E as, e.g., JET due to the small heating power to density ratio in W7-X. The best performing W7-AS discharge [57] (red + yellow bold cross) was achieved in a so-called high confinement NBI discharge which has strong similarities to the W7-X scenario described here [58–60] and the scaling from this to the high performance W7-X plasma follows the same scaling

as in tokamak H-mode plasmas. This is in line with a more detailed comparison done in [54] where it has been shown as well that the empirical stellarator scaling ISS04 [49] can be applied to tokamaks. The ISS04 scaling is gyro-Bohm-like but additionally includes an ι factor. As ι is smaller in all presented tokamaks than in W7-X (due to current stability limits) the cloud of data points move relatively to each other which can be seen in the middle plot of Fig. 2. But this does not change the conclusion, that, given the machine parameters, W7-X not only achieved a triple product comparable to the *H*-mode tokamak performance but also the energy confinement time and its scaling is compatible with tokamak *H*-mode data. The improvement in the core ion temperature going from W7-AS to W7-X is very well captured by the tokamak fitted gyro-Bohm scaling as can be seen on the right-hand side of Fig. 2. Only noninductive tokamak *H*-mode scenarios (black bordered points) systematically stray below the gyro-Bohm fit as is for example seen in low-density EAST plasmas [61] where the focus is on steady-state operation rather than high confinement. Extrapolating the presented gyro-Bohm scaling to reactor dimensions, without implying W7-X would simply extrapolate to a reactor, gives a central ion temperature of about 15 keV (HELIAS point, marked as blue cross), matching that shown with one-dimensional (1D) transport simulations to be needed to produce fusion power on the order of 3 GW [62]. However, any attempt at progressing towards a stellarator fusion reactor based on the shown W7-X data points requires a plasma regime where the density peaking can be held stable in order to take advantage of the resulting turbulence suppression in the steady state. The reported record performance was achieved by mixed NBI and ECR heating to create the necessary density profile.

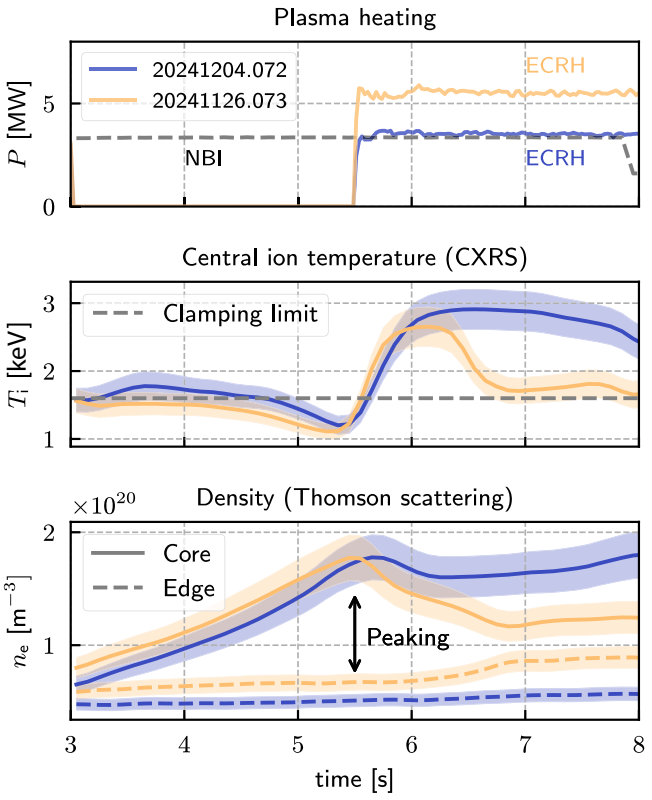


FIG. 3. Plasma and heating parameters for the presented record discharge (No. 20241204.072, blue lines) and another plasma discharge with a similar heating scenario (No. 20241126.073, orange lines). Top: NBI and ECR heating power time traces. Middle: Time traces of measured central ion temperature. Bottom: Time traces of measured core and edge ($r/a = 0.8$) electron density. The distance between the core and edge lines represents the density peaking.

IV. EXPERIMENTAL SCENARIO

In Fig. 3 the plasma and heating parameters are shown for the presented record discharge (No. 20241204.072, blue lines) and another plasma discharge with a similar heating scenario (No. 20241126.073, orange lines). During an initial pure NBI heating phase (top plot) the core electron density and therefore the density peaking continuously increases (bottom plot). The reintroduction of ECRH at 5.5 s after the core density gradient has developed has two effects: Firstly, it raises the ion temperature above the clamping limit (middle plot) due to the reduced turbulent heat transport [23], and second, the density peaking rate is reduced (bottom plot) due to an induced core density *pump-out* effect. It can be seen from No. 20241126.073 (orange lines) that applying too much ECRH leads to a reduction of the total density peaking and eventually to a loss of the improved energy confinement reflected by the sudden decrease of the central ion temperature around 6.5 s. Therefore, a key experimental achievement which led to the record triple product was the successful fine tuning of the ECRH parameters (power, reintroduction time, frequency, stability) in order to stabilize the core electron density gradient while simultaneously maximizing the central ion temperature, as can be seen for No. 20241204.072 from 6 to 8 s which represents the HP phase of the discharge. In contrast to tokamaks, where the pump-out effect has been investigated in detail [63–67], it is not yet well understood in W7-X. Experimentally, it was observed to be proportional to the reintroduced ECRH power and dependent on the magnetic configuration which differ in magnetic mirror ratio m_r, ι profile, and volume, but could not yet be ascribed to a single physics phenomenon. Consequently, while the improved confinement in the presence of peaked density profiles was seen across the whole magnetic configuration space, the maximal achievable stable performance differed between the explored configurations (details can be found in Appendix B). The slight decay of the central ion temperature during the HP phase (6 to 8 s) seen for No. 20241204.072 (middle plot, blue line) is due to a slow accumulation of impurities that is a consequence of the particle transport [31]. This may become a significant problem at much longer periods, especially if impurity seeding is used to mitigate divertor heat loads [68,69], making impurity transport in reduced turbulence scenarios a focus in future W7-X experiments as well as for stellarator optimization.

V. CONCLUSION

In Wendelstein 7-X an exceptional stellarator plasma performance in terms of the triple product was measured. The achieved value is comparable to *H*-mode tokamak discharges

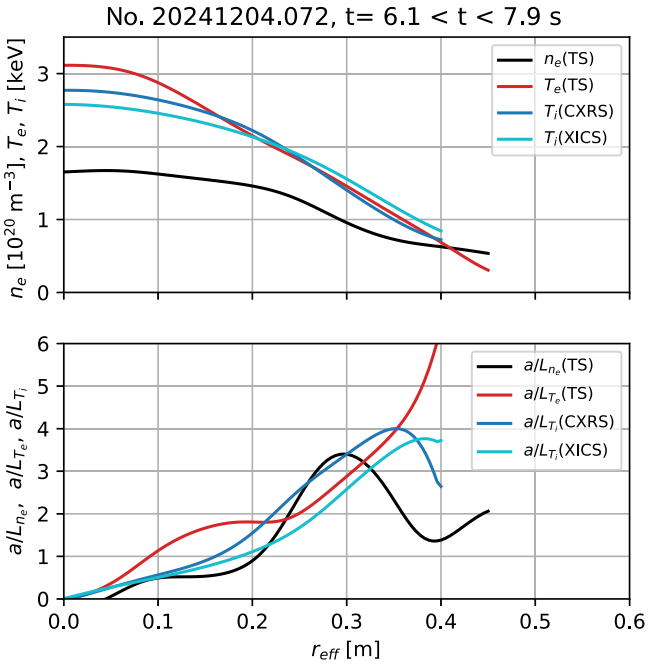


FIG. 4. Plasma profiles and normalised gradients in a FMM* configuration (No. 20241204.072) in the HP phase between 6.1 and 7.9 s.

when taking into account the differing stored magnetic energy of the devices. Comparing to a similar high confinement discharge scenario from W7-AS [57,60], good agreement with the reactor favorable gyro-Bohm scaling was found. The measured energy confinement time was above the ISS04 scaling for several energy confinements times. While the improved confinement is a robust effect of the core density gradient, only careful optimization of the ECRH reintroduction parameters and magnetic configuration made it possible to maximize the triple product and simultaneously stabilize the density gradient to finally lead to this result.

ACKNOWLEDGMENTS

The authors want to thank Ulrich Stroth for helpful discussions on the manuscript. The authors thank Xavier Litaudon and the whole CICLOP group for assembling the CICLOP database and giving the permission to use it. This work has been carried out within the framework of the EUROfusion Consortium, funded by the European Union via the Euratom Research and Training Programme (Grant Agreement No. 101052200 — EUROfusion). Views and opinions expressed are however those of the author(s) only and do not necessarily reflect those of the European Union or the European Commission. Neither the European Union nor the European Commission can be held responsible for them.

Conceptualization: O.F., S.A.B., A.L., T.S., R.L.-C., and S.B; Investigation + Data Curation: O.F., T.S., A.L., R.L.-C, S.B., J.B., G.F., T.G., M.W., D.H., J.K., H.L., P.M., N.P., E.P., P.P., K.R., and N.R.; Methodology: S.B., O.F., and S.A.B.; Writing original draft & Visualization: S.B.; Writing review and editing: O.F. and S.A.B.; Project administration: R.C.W.; Software & Resources: W7-X Team (see the Supplemental Material [70]).

DATA AVAILABILITY

The data that support the findings of this article are not publicly available because of legal restrictions preventing unrestricted public distribution. The data are available from the authors upon reasonable request.

APPENDIX A: PLASMA PROFILES IN NO. 20241204.072

The electron density and temperature profiles were obtained using the Thomson scattering diagnostic [71]. The electron density profile was renormalized using the line integrated density provided by the interferometer system [72]. Ion temperature profiles were obtained using the charge-exchange recombination spectroscopy system (CXRS) [73] and the X-Ray imaging crystal spectrometer (XICS) [74], corrected according to Ref. [75]. The profile mapping was done using VMEC [76,77] runs with consistent pressure profiles, thereby including β effects on the equilibrium. The plasma profiles and normalized gradient lengths for discharge No. 20241204.072 in the high-performance phase are shown in Fig. 4.

APPENDIX B: EXPERIMENTAL PLASMA PERFORMANCE OPTIMIZATION IN DIFFERENT MAGNETIC CONFIGURATIONS

ECRH powers of between 2.5 and 5.5 MW were introduced to plasmas with 3.5 MW of NBI after the density gradient had developed to just below the O2 ECRH cutoff density, while optimizing the magnetic field strength to maintain on-axis deposition of the ECRH during the highest β phase. Similar power scans were performed in each of the main W7-X magnetic configurations which differ in magnetic mirror ratio m_r, ι profile, and volume. Table II lists the configurations used along with the ECRH power required to hold the density peaking stable, determined from the trend of density rise rate to ECRH power. The peak plasma parameters achieved at the most stable executed plasma are also given.

The high- and low-mirror configurations perform the worst, allowing the lowest reintroduced ECRH power due to a strong pump-out effect, which, together with a poorer confinement in the reduced turbulence phase [78], results in an ion temperature barely above the clamping limit. The lowest pump-out effect and hence highest balance power is seen in a configuration belonging to a fine scan of iota [79], named FMM, which forms a limiter plasma and has the largest volume, as the resonant 5/5 islands that would otherwise form the divertor are pushed inside the plasma boundary. Reducing the size of these islands using the control coils resulted in the magnetic configuration FMM* in which the here presented record performance was achieved.

TABLE II. Experimentally determined ECRH pump-out balance for two NBI sources (3.5 MW) in several magnetic configurations and the best achieved core plasma parameters. Note that a final optimization of T_i, W_{dia}, and τ_E was completed only for Standard (EIM) and iota scan (FMM) configurations.

Configuration	ι	m_r (10^{-2})	a (m)	P_{ECRH} steady (MW)	T_i (keV)	W_{dia} (MJ)	τ_E (ms)	Program ID
Low mirror (AIM)	0.84	0.01	0.53	1.5	1.6	0.8	180	20230316.069
High mirror (KKM)	0.87	10.1	0.51	1.5	1.6	0.8	180	20250227.082
Standard (EIM)	0.85	4.34	0.52	2.0	2.6	1.2	180	20241205.066
High iota (FTM)	1.01	5.44	0.48	3.0	2.1	1.2	150	20241022.039
Iota scan, limiter with internal islands (FMM)	0.91	4.72	0.55	3.5	2.3	1.2	170	20241204.063
Iota scan, limiter with suppressed islands (FMM*)	0.91	4.72	0.55	3.5	2.9	1.8	260	20241204.072

APPENDIX C: GYRO-BOHM SCALING

Assuming dominant heat transport gyro-Bohm scaling in ρ^* (ITG) and weak dependence on β and ν^* as in the tokamak H mode [50],

$$\omega\tau_{E,\mathrm{gB}} \propto (\rho^*)^{-3}, \tag{C1}$$

$$\omega = \frac{qB}{2\pi m}, \tag{C2}$$

$$\rho^* = \frac{\rho_L}{a} = \frac{mv_\perp}{a\cdot qB} = \frac{(2kTm)^{\frac{1}{2}}}{a\cdot qB}, \tag{C3}$$

$$v_\perp = \frac{2}{3}v_{\mathrm{th}}, \tag{C4}$$

$$\tau_{E,\mathrm{gB}} \propto \frac{1}{\omega}\left(\frac{(2kTm)^{\frac{1}{2}}}{a\cdot qB}\right)^{-3} \propto m^{-\frac{1}{2}}T^{-\frac{3}{2}}a^3q^2B^2, \tag{C5}$$

where ω is the gyrofrequency, q the particle charge, m the mass, ρ_L the gyroradius, a the minor radius, T the temperature, B the magnetic field strength on axis, and τ the energy confinement time. Combining with the definition of τ_E via the kinetic profiles and heating power,

$$\tau_E = \frac{W}{P_{\mathrm{H}}} = \frac{3nkT}{P_{\mathrm{H}}}, \tag{C6}$$

gyro-Bohm scalings for T and τ_E can be written in terms of geometric quantities, density n, and heating power P_{H}:

$$T_{\mathrm{gB}} = c_1\epsilon^{0.4}m^{-0.2}\left(\frac{P_{\mathrm{H}}}{n}\right)^{0.4}B^{0.8}, \tag{C7}$$

$$\tau_{E,\mathrm{gB}} = c_2a^3\epsilon^{-0.6}m^{-0.2}\left(\frac{P_{\mathrm{H}}}{n}\right)^{-0.6}B^{0.8}. \tag{C8}$$

Consequently, if gyro-Bohm scaling holds, the triple product F scales as

$$F \propto a^3\epsilon^{-0.2}m^{-0.4}n^{1.2}P_{\mathrm{H}}^{-0.2}B^{1.6}. \tag{C9}$$

[1] J. D. Lawson, Some criteria for a power producing thermonuclear reactor, Proc. Phys. Soc. B **70**, 6 (1957).

[2] S. E. Wurzel and S. C. Hsu, Progress toward fusion energy breakeven and gain as measured against the Lawson criterion, Phys. Plasmas **29**, 062103 (2022).

[3] JET Team, Fusion energy production from a deuterium-tritium plasma in the JET tokamak, Nucl. Fusion **32**, 187 (1992).

[4] M. Greenwald, Density limits in toroidal plasmas, Plasma Phys. Controlled Fusion **44**, R27 (2002).

[5] P. Helander, C. D. Beidler, T. M. Bird, M. Drevlak, Y. Feng, R. Hatzky, F. Jenko, R. Kleiber, J. H. E. Proll, Y. Turkin, and P. Xanthopoulos, Stellarator and tokamak plasmas: A comparison, Plasma Phys. Controlled Fusion **54**, 124009 (2012).

[6] F. Wagner, Stellarators and optimised stellarators, Fusion Technol. **33**, 67 (1998).

[7] H. Maassberg, R. Brakel, R. Burhenn, U. Gasparino, P. Grigull, M. Kick, G. Kuhner, H. Ringler, F. Sardei, U. Stroth, and A. Weller, Transport in stellarators, Plasma Phys. Controlled Fusion **35**, B319 (1993).

[8] G. Grieger and I. Milch, Das Fusionsexperiment WENDELSTEIN 7-X, Phys. Bl. **49**, 1001 (1993).

[9] R. Wolf, T. Andreeva, S. Bozhenkov, C. Brandt, R. Burhenn, B. Buttenschön, G. Fuchert, B. Geiger, O. Grulke, H. Laqua, N. Pablant, K. Rahbarnia, T. Stange, A. von Stechow, N. Tamura, H. Thomsen, Y. Turkin, T. Wegner, I. Abramovic, S. Äkäslompolo, *et al.*, Major results from the first plasma campaign of the Wendelstein 7-X stellarator, Nucl. Fusion **57**, 102020 (2017).

[10] T. Klinger, A. Alonso, S. Bozhenkov, R. Burhenn, A. Dinklage, G. Fuchert, J. Geiger, O. Grulke, A. Langenberg, M. Hirsch, G. Kocsis, J. Knauer, A. Krämer-Flecken, H. Laqua, S. Lazerson, M. Landreman, H. Maaßberg, S. Marsen, M. Otte, N. Pablant, *et al.*, Performance and properties of the first plasmas of Wendelstein 7-X, Plasma Phys. Controlled Fusion **59**, 014018 (2017).

[11] C. Beidler, G. Grieger, F. Herrnegger, E. Harmeyer, J. Kisslinger, W. Lotz, H. Maassberg, P. Merkel, J. Nuehrenberg, F. Rau, J. Sapper, F. Sardei, R. Scardovelli, A. Schlueter, and H. Wobig, Physics and engineering design for Wendelstein VII-X, Fusion Technol. **17**, 148 (1990).

[12] C. D. Beidler, H. M. Smith, A. Alonso, T. Andreeva, J. Baldzuhn, M. N. A. Beurskens, M. Borchardt, S. A. Bozhenkov,

K. J. Brunner, H. Damm, M. Drevlak, O. P. Ford, G. Fuchert, J. Geiger, P. Helander, U. Hergenhahn, M. Hirsch, U. Höfel, Y. O. Kazakov, R. Kleiber, *et al.*, Demonstration of reduced neoclassical energy transport in Wendelstein 7-X, Nature (London) **596**, 221 (2021).

[13] M. Beurskens, S. Bozhenkov, O. Ford, P. Xanthopoulos, A. Zocco, Y. Turkin, A. Alonso, C. Beidler, I. Calvo, D. Carralero, T. Estrada, G. Fuchert, O. Grulke, M. Hirsch, K. Ida, M. Jakubowski, C. Killer, M. Krychowiak, S. Kwak, S. Lazerson, *et al.*, Ion temperature clamping in Wendelstein 7-X electron cyclotron heated plasmas, Nucl. Fusion **61**, 116072 (2021).

[14] M. Beurskens, C. Angioni, S. A. Bozhenkov, O. Ford, C. Kiefer, P. Xanthopoulos, Y. Turkin, J. Alcusón, J. Baehner, C. Beidler, G. Birkenmeier, E. Fable, G. Fuchert, B. Geiger, O. Grulke, M. Hirsch, M. Jakubowski, H. Laqua, A. Langenberg, S. Lazerson, *et al.*, Confinement in electron heated plasmas in Wendelstein 7-X and ASDEX upgrade; the necessity to control turbulent transport, Nucl. Fusion **62**, 016015 (2022).

[15] W. Horton, *Turbulent Transport in Magnetized Plasmas* (World Scientific, Singapore, 2012).

[16] P. Xanthopoulos *et al.*, Turbulence mechanisms of enhanced performance stellarator plasmas, Phys. Rev. Lett. **125**, 075001 (2020).

[17] J. H. E. Proll, P. Helander, J. W. Connor, and G. G. Plunk, Resilience of quasi-isodynamic stellarators against trapped-particle instabilities, Phys. Rev. Lett. **108**, 245002 (2012).

[18] G. G. Plunk, P. Xanthopoulos, G. M. Weir, S. A. Bozhenkov, A. Dinklage, G. Fuchert, J. Geiger, M. Hirsch, U. Hoefel, M. Jakubowski, A. Langenberg, N. Pablant, E. Pasch, T. Stange, D. Zhang, and the W7-X Team, Stellarators resist turbulent transport on the electron Larmor scale, Phys. Rev. Lett. **122**, 035002 (2019).

[19] J. A. Alcusón, P. Xanthopoulos, G. G. Plunk, P. Helander, F. Wilms, Y. Turkin, A. von Stechow, and O. Grulke, Suppression of electrostatic micro-instabilities in maximum-J stellarators, Plasma Phys. Controlled Fusion **62**, 035005 (2020).

[20] S. Bozhenkov, Y. Kazakov, O. Ford, M. Beurskens, J. Alcusón, J. Alonso, J. Baldzuhn, C. Brandt, K. Brunner, H. Damm, G. Fuchert, J. Geiger, O. Grulke, M. Hirsch, U. Höfel, Z. Huang, J. Knauer, M. Krychowiak, A. Langenberg, H. Laqua, *et al.*, High-performance plasmas after pellet injections in Wendelstein 7-X, Nucl. Fusion **60**, 066011 (2020).

[21] T. Klinger, T. Andreeva, S. Bozhenkov, C. Brandt, R. Burhenn, B. Buttenschön, G. Fuchert, B. Geiger, O. Grulke, H. Laqua, N. Pablant, K. Rahbarnia, T. Stange, A. von Stechow, N. Tamura, H. Thomsen, Y. Turkin, T. Wegner, I. Abramovic, S. Äkäslompolo, *et al.*, Overview of first Wendelstein 7-X high-performance operation, Nucl. Fusion **59**, 112004 (2019).

[22] J. Baldzuhn *et al.*, Enhanced energy confinement after series of pellets in Wendelstein 7-X, Plasma Phys. Controlled Fusion **62**, 055012 (2020).

[23] O. Ford, M. Beurskens, S. Bozhenkov, S. Lazerson, L. Vanó, A. Alonso, J. Baldzuhn, C. Beidler, C. Biedermann, R. Burhenn, G. Fuchert, D. Hartmann, M. Hirsch, A. Langenberg, H. Laqua, P. McNeely, N. Pablant, E. Pasch, F. Reimold, T. Romba, *et al.*, Turbulence-reduced high-performance scenarios in Wendelstein 7-X, Nucl. Fusion **64**, 086067 (2024).

[24] P. McNeely, M. Barlak, J. Baldzuhn, S. Bozhenkov, M. Drevlak, G. Gawlik, B. Heinemann, D. Holtum, J. Jagielski, R. Kairys, R. Nocentini, R. Riedl, P. Rong, N. Rust, R. Schroeder, E. Speth, A. Stäbler, A. Turos, and R. Wolf, Current status of the neutral beam heating system of W7-X, Fusion Eng. Des. **88**, 1034 (2013).

[25] S. A. Lazerson, O. Ford, S. Äkaslompolö, S. Bozhenkov, C. Slaby, L. Vanó, A. Spanier, P. McNeely, N. Rust, D. Hartmann, P. Poloskei, B. Buttenschön, R. Burhenn, N. Tamura, R. Bussiahn, T. Wegner, M. Drevlak, Y. Turkin, K. Ogawa, J. Knauer, *et al.*, First neutral beam experiments on Wendelstein 7-X, Nucl. Fusion **61**, 096008 (2021).

[26] S. A. Lazerson, O. P. Ford, C. Nuehrenberg, S. Äkäslompolo, P. Z. Poloskei, M. Machielsen, P. McNeely, L. Vanó, N. Rust, S. Bozhenkov, T. W. Neelis, J. P. Graves, D. Pfefferlé, A. Spanier, D. Hartmann, N. Marushchenko, Y. Turkin, M. Hirsch, N. Chaudhary, U. Hoefel, *et al.*, Validation of the BEAMS3D neutral beam deposition model on Wendelstein 7-X, Nucl. Fusion **60**, 076020 (2020).

[27] H. Thienpondt, J. M. García-Regaña, I. Calvo, J. A. Alonso, J. L. Velasco, A. González-Jerez, M. Barnes, K. Brunner, O. Ford, G. Fuchert, J. Knauer, E. Pasch, L. Vanó, and The Wendelstein 7-X Team, Prevention of core particle depletion in stellarators by turbulence, Phys. Rev. Res. **5**, L022053 (2023).

[28] S. Bannmann, O. Ford, U. Hoefel, P. Poloskei, A. Pavone, S. Kwak, J. Svensson, S. Lazerson, P. McNeely, N. Rust, D. Hartmann, E. Pasch, G. Fuchert, R. Wolf, and the W7-X-Team, Fast forward modeling of neutral beam injection and halo formation including full Balmer-α emission prediction at W7-X, J. Instrum. **18**, P10029 (2023).

[29] D. Carralero, T. Estrada, E. Maragkoudakis, T. Windisch, J. Alonso, M. Beurskens, S. Bozhenkov, I. Calvo, H. Damm, O. Ford, G. Fuchert, J. García-Regaña, N. Pablant, E. Sánchez, E. Pasch, J. Velasco, and the Wendelstein 7-X team, An experimental characterization of core turbulence regimes in Wendelstein 7-X, Nucl. Fusion **61**, 096015 (2021).

[30] A. v. Stechow, O. Grulke, T. Wegner, J. H. E. Proll, J. A. Alcusón, H. M. Smith, J. Baldzuhn, C. D. Beidler, M. N. A. Beurskens, S. A. Bozhenkov, E. Edlund, B. Geiger, Z. Huang, O. P. Ford, G. Fuchert, A. Langenberg, N. Pablant, E. Pasch, M. Porkolab, K. Rahbarnia, *et al.*, Suppression of core turbulence by profile shaping in Wendelstein 7-X, arXiv:2010.02160.

[31] T. Romba, F. Reimold, R. Jaspers, O. Ford, L. Vanó, T. Klinger, and the W7-X Team, Suppression of anomalous impurity transport in NBI-heated W7-X plasmas, Nucl. Fusion **63**, 076023 (2023).

[32] T. Romba, F. Reimold, S. Bannmann, T. Bleher, O. Ford, P. Z. Poloskei, and M. Wappl, The suppression of anomalous impurity transport above a critical normalized density gradient scale length in Wendelstein 7-X, Plasma Phys. Controlled Fusion **67**, 065016 (2025).

[33] S. A. Bozhenkov, O. P. Ford, M. Wappl, S. Bannmann, T. Romba, V. Perseo, K. Aleynikova, D. Zhang, I. Amri, J.-P. Bäehner, J. Baldzuhn, L. R. Baylor, Y. Boumendjel, C. Brandt, K. J. Brunner, C. Büschel, D. Carralero, A. Dinklage, T. Estrada, G. Fuchert, *et al.*, Routes to high-performance operation in Wendelstein 7-X: turbulence suppression with shaping of the density profile, Plasma Phys. Controlled Fusion **68**, 055015 (2026).

[34] J. Lion, J.-C. Anglès, L. Bonauer, A. Bañón Navarro, S. Cadena Ceron, R. Davies, M. Drevlak, N. Foppiani, J. Geiger, A. Goodman, W. Guo, E. Guiraud, F. Hernández, S. Henneberg, R. Herrero, C. Hintze, H. Höchter, J. Jelonnek, F. Jenko, R. Jorge,

et al., Stellaris: A high-field quasi-isodynamic stellarator for a prototypical fusion power plant, Fusion Eng. Des. **214**, 114868 (2025).

[35] G. G. Plunk, A. G. Goodman, P. Xanthopoulos, P. Costello, H. M. Smith, K. Aleynikova, C. D. Beidler, M. Drevlak, and P. Helander, Enhanced performance in quasi-isodynamic max-J stellarators with a turbulent particle pinch, Phys. Rev. E **113**, 045215 (2026).

[36] D. L. C. Agapito Fernando, A. Bañón Navarro, D. Carralero, A. Alonso, A. Di Siena, J. L. Velasco, F. Wilms, G. Merlo, F. Jenko, S. A. Bozhenkov, E. Pasch, G. Fuchert, K. J. Brunner, J. Knauer, A. Langenberg, N. A. Pablant, T. Gonda, O. P. Ford, L. Vanó, T. Windisch, *et al.*, Validation of a comprehensive first-principles-based framework for predicting the performance of future stellarators, Phys. Plasmas **32**, 073904 (2025).

[37] H. Cu-Castillo, A. B. Navarro, G. Merlo, F. Reimold, T. Romba, O. Ford, S. Bannmann, L. Vanó, M. Wappl, J. Geiger, A. Zocco, F. Jenko, and W7X-Team, Microtearing turbulence and its role in high-density-gradient plasmas in Wendelstein 7-X, Phys. Rev. Lett. (2026).

[38] X. Litaudon, H.-S. Bosch, T. Morisaki, M. Barbarino, A. Bock, E. Belonohy, S. Brezinsek, J. Bucalossi, S. Coda, R. Daniel, A. Ekedahl, K. Hanada, C. Holcomb, J. Huang, S. Ide, M. Jakubowski, B. V. Kuteev, E. Lerche, T. Luce, P. Maget, *et al.*, Long plasma duration operation analyses with an international multi-machine (tokamaks and stellarators) database, Nucl. Fusion **64**, 015001 (2024).

[39] F. Wagner, J. Baldzuhn, R. Brakel, R. Burhenn, V. Erckmann, T. Estrada, P. Grigull, H. J. Hartfuss, G. Herre, M. Hirsch, J. V. Hofmann, R. Jaenicke, A. Rudyj, U. Stroth, and A. Weller, H-mode of W7-AS stellarator, Plasma Phys. Controlled Fusion **36**, A61 (1994).

[40] ITER Physics Expert Group on Confinement and Transport, ITER Physics Expert Group on Confinement Modelling and Database, and ITER Physics Basis Editors, Chapter 2: Plasma confinement and transport, Nucl. Fusion **39**, 2175 (1999).

[41] A. Bock, E. Fable, R. Fischer, M. Reich, D. Rittich, J. Stober, M. Bernert, A. Burckhart, H. Doerk, M. Dunne, B. Geiger, L. Giannone, V. Igochine, A. Kappatou, R. McDermott, A. Mlynek, T. Odstrčil, G. Tardini, H. Zohm, and The ASDEX upgrade Team, Non-inductive improved H-mode operation at ASDEX upgrade, Nucl. Fusion **57**, 126041 (2017).

[42] X. Litaudon, A. Bécoulet, F. Crisanti, R. Wolf, Y. Baranov, E. Barbato, M. Bécoulet, R. Budny, C. Castaldo, R. Cesario, C. Challis, G. Conway, M. D. Baar, P. D. Vries, R. Dux, L. Eriksson, B. Esposito, R. Felton, C. Fourment, D. Frigione, *et al.*, Progress towards steady-state operation and real-time control of internal transport barriers in JET, Nucl. Fusion **43**, 565 (2003).

[43] A. M. Garofalo, E. J. Doyle, J. R. Ferron, C. M. Greenfield, R. J. Groebner, A. W. Hyatt, G. L. Jackson, R. J. Jayakumar, J. E. Kinsey, R. J. La Haye, G. R. McKee, M. Murakami, M. Okabayashi, T. H. Osborne, C. C. Petty, P. A. Politzer, H. Reimerdes, J. T. Scoville, W. M. Solomon, H. E. St. John, *et al.*, Access to sustained high-beta with internal transport barrier and negative central magnetic shear in DIII-D, Phys. Plasmas **13**, 056110 (2006).

[44] B. Wan, Y. Liang, X. Gong, N. Xiang, G. Xu, Y. Sun, L. Wang, J. Qian, H. Liu, L. Zeng, L. Zhang, X. Zhang, B. Ding, Q. Zang, B. Lyu, A. Garofalo, A. Ekedahl, M. Li, F. Ding, S. Ding, *et al.*, Recent advances in EAST physics experiments in support of steady-state operation for ITER and CFETR, Nucl. Fusion **59**, 112003 (2019).

[45] O. Grulke, C. Albert, J. Alcuson Belloso, P. Aleynikov, K. Aleynikova, A. Alonso, G. Anda, T. Andreeva, M. Arvanitou, E. Ascasibar, E. Aymerich, K. Avramidis, J.-P. Bähner, S.-G. Baek, M. Balden, J. Baldzuhn, S. Ballinger, M. Banduch, S. Bannmann, A. Bañón Navarro, *et al.*, Overview of the first Wendelstein 7-X long pulse campaign with fully water-cooled plasma facing components, Nucl. Fusion **64**, 112002 (2024).

[46] K. Rahbarnia, H. Thomsen, U. Neuner, J. Schilling, J. Geiger, G. Fuchert, T. Andreeva, M. Endler, D. Hathiramani, T. Bluhm, M. Zilker, B. Carvalho, A. Werner, and Wendelstein 7-X Team, Diamagnetic energy measurement during the first operational phase at the Wendelstein 7-X stellarator, Nucl. Fusion **58**, 096010 (2018).

[47] A. Pavone, U. Hergenhahn, M. Krychowiak, U. Hoefel, S. Kwak, J. Svensson, P. Kornejew, V. Winters, R. Koenig, M. Hirsch, K.-J. Brunner, E. Pasch, J. Knauer, G. Fuchert, E. Scott, M. Beurskens, F. Effenberg, D. Zhang, O. Ford, L. Vanó, *et al.*, Measurements of visible bremsstrahlung and automatic Bayesian inference of the effective plasma charge Z_{eff} at W7-X, J. Instrum. **14** (10), C10003.

[48] T. Romba, Validation of the W7-X CXRS for impurity density profiles, Master's thesis, Eindhoven University of Technology, 2021, https://research.tue.nl/en/studentTheses/validation-of-the-w7-x-cxrs-for-impurity-density-profiles.

[49] H. Yamada, J. Harris, A. Dinklage, E. Ascasibar, F. Sano, S. Okamura, J. Talmadge, U. Stroth, A. Kus, S. Murakami, M. Yokoyama, C. Beidler, V. Tribaldos, K. Watanabe, and Y. Suzuki, Characterization of energy confinement in net-current free plasmas using the extended International Stellarator Database, Nucl. Fusion **45**, 1684 (2005).

[50] J. Cordey, K. Thomsen, A. Chudnovskiy, O. Kardaun, T. Takizuka, J. Snipes, M. Greenwald, L. Sugiyama, F. Ryter, A. Kus, J. Stober, J. DeBoo, C. Petty, G. Bracco, M. Romanelli, Z. Cui, Y. Liu, D. McDonald, A. Meakins, Y. Miura, *et al.*, Scaling of the energy confinement time with β and collisionality approaching ITER conditions, Nucl. Fusion **45**, 1078 (2005).

[51] A. Dinklage, E. Ascasíbar, C. D. Beidler, R. Brakel, J. Geiger, J. H. Harris, A. Kus, S. Murakami, S. Okamura, R. Preuss, F. Sano, U. Stroth, Y. Suzuki, J. Talmadge, V. Tribaldos, K. Y. Watanabe, A. Weller, H. Yamada, and M. Yokoyama, Assessment of global stellarator confinement: Status of the International stellarator confinement database, Fusion Sci. Technol. **51**, 1 (2007).

[52] J. Miyazawa, H. Yamada, R. Sakamoto, H. Funaba, K. Y. Watanabe, S. Sakakibara, K. Ida, M. Goto, T. Morisaki, S. Murakami, S. Inagaki, and LHD Experiment Group, Characteristics of the global energy confinement and central pressure in LHD, Fusion Sci. Technol. **58**, 29 (2010).

[53] G. Manfredi and M. Ottaviani, Gyro-Bohm scaling of ion thermal transport from global numerical simulations of ion-temperature-gradient-driven turbulence, Phys. Rev. Lett. **79**, 4190 (1997).

[54] U. Stroth, G. Fuchert, M. Beurskens, G. Birkenmeier, P. Schneider, E. Scott, K. Brunner, F. Günzkofer, P. Hacker, O. Kardaun, J. Knauer, K. Rahbarnia, D. Zhang, and MST1 team, Stellarator-tokamak energy confinement comparison based on

ASDEX upgrade and Wendelstein 7-X hydrogen plasmas, Nucl. Fusion **61**, 016003 (2021).

[55] U. Stroth, M. Murakami, R. Dory, H. Yamada, S. Okamura, F. Sano, and T. Obiki, Energy confinement scaling from the International stellarator database, Nucl. Fusion **36**, 1063 (1996).

[56] F. Warmer, C. D. Beidler, A. Dinklage, R. Wolf, and The W7-X Team, From W7-X to a HELIAS fusion power plant: Motivation and options for an intermediate-step burning-plasma stellarator, Plasma Phys. Controlled Fusion **58**, 074006 (2016).

[57] F. Wagner, S. Bäumel, J. Baldzuhn, N. Basse, R. Brakel, R. Burhenn, A. Dinklage, D. Dorst, H. Ehmler, M. Endler, V. Erckmann, Y. Feng, F. Gadelmeier, J. Geiger, L. Giannone, P. Grigull, H.-J. Hartfuss, D. Hartmann, D. Hildebrandt, M. Hirsch, *et al.*, W7-AS: One step of the Wendelstein stellarator line, Phys. Plasmas **12**, 072509 (2005).

[58] U. Stroth, J. Baldzuhn, J. Geiger, T. Geist, L. Giannone, H.-J. Hartfuß, M. Hirsch, R. Jaenicke, M. Kick, J. P. Koponen, G. Kühner, F.-P. Penningsfeld, F. Wagner, and the W7-AS Team, High-confinement NBI discharges in the W7-AS stellarator, Plasma Phys. Controlled Fusion **40**, 1551 (1998).

[59] M. Kick, H. Maaßberg, M. Anton, J. Baldzuhn, M. Endler, C. Görner, M. Hirsch, A. Weller, S. Zoletnik, and the W7-AS Team, Electric field and transport in W7-AS, Plasma Phys. Controlled Fusion **41**, A549 (1999).

[60] M. Hirsch, J. Baldzuhn, C. Beidler, R. Brakel, R. Burhenn, A. Dinklage, H. Ehmler, M. Endler, V. Erckmann, Y. Feng, J. Geiger, L. Giannone, G. Grieger, P. Grigull, H.-J. Hartfuß, D. Hartmann, R. Jaenicke, R. König, H. P. Laqua, H. Maaßberg, *et al.*, Major results from the stellarator Wendelstein 7-AS, Plasma Phys. Controlled Fusion **50**, 053001 (2008).

[61] J. S. Hu, Z. Sun, H. Y. Guo, J. G. Li, B. N. Wan, H. Q. Wang, S. Y. Ding, G. S. Xu, Y. F. Liang, D. K. Mansfield, R. Maingi, X. L. Zou, L. Wang, J. Ren, G. Z. Zuo, L. Zhang, Y. M. Duan, T. H. Shi, L. Q. Hu, and East team, New steady-state quiescent high-confinement plasma in an experimental advanced superconducting tokamak, Phys. Rev. Lett. **114**, 055001 (2015).

[62] F. Warmer, C. D. Beidler, A. Dinklage, Y. Turkin, and R. Wolf, Limits of confinement enhancement for stellarators, Fusion Sci. Technol. **68**, 727 (2015).

[63] C. Angioni, A. G. Peeters, G. V. Pereverzev, F. Ryter, G. Tardini (ASDEX Upgrade Team), Density peaking, anomalous pinch, and collisionality in tokamak plasmas, Phys. Rev. Lett. **90**, 205003 (2003).

[64] C. Angioni, A. Peeters, X. Garbet, A. Manini, F. Ryter, and ASDEX upgrade team, Density response to central electron heating: Theoretical investigations and experimental observations in ASDEX upgrade, Nucl. Fusion **44**, 827 (2004).

[65] C. Angioni, E. Fable, M. Greenwald, M. Maslov, A. G. Peeters, H. Takenaga, and H. Weisen, Particle transport in tokamak plasmas, theory and experiment, Plasma Phys. Controlled Fusion **51**, 124017 (2009).

[66] X. Wang, S. Mordijck, E. Doyle, T. Rhodes, L. Zeng, G. McKee, M. Austin, O. Meneghini, G. Staebler, and S. Smith, Understanding ECH density pump-out in DIII-D H-mode plasmas, Nucl. Fusion **57**, 116046 (2017).

[67] A. Zabolotsky, H. Weisen, and TCV Team, Density profile peaking in the presence of ECRH heating in TCV, Plasma Phys. Controlled Fusion **48**, 369 (2006).

[68] F. Effenberg, S. Brezinsek, Y. Feng, R. König, M. Krychowiak, M. Jakubowski, H. Niemann, V. Perseo, O. Schmitz, D. Zhang, T. Barbui, C. Biedermann, R. Burhenn, B. Buttenschön, G. Kocsis, A. Pavone, F. Reimold, T. Szepesi, H. Frerichs, Y. Gao, *et al.*, First demonstration of radiative power exhaust with impurity seeding in the island divertor at Wendelstein 7-X, Nucl. Fusion **59**, 106020 (2019).

[69] Y. Gao, J. Geiger, M. W. Jakubowski, A. Pandey, S. Bozhenkov, Y. Feng, M. Endler, J. Baldzuhn, V. Perseo, T. Kremeyer, G. Schlisio, A. Puig Sitjes, M. Otte, D. Naujoks, M. Krychowiak, R. König, D. Zhang, T. Szepesi, G. Kocsis, G. Cseh, *et al.*, Heat and particle exhaust in high-performance plasmas in Wendelstein 7-X, Nucl. Fusion **64**, 076060 (2024).

[70] See Supplemental Material http://link.aps.org/supplemental/10.1103/q59k-8m26 for the members of the W7-X Team.

[71] S. Bozhenkov, M. Beurskens, A. D. Molin, G. Fuchert, E. Pasch, M. Stoneking, M. Hirsch, U. Höfel, J. Knauer, J. Svensson, H. T. Mora, and R. Wolf, The Thomson scattering diagnostic at Wendelstein 7-X and its performance in the first operation phase, J. Instrum. **12** (10), P10004.

[72] K. Brunner, T. Akiyama, M. Hirsch, J. Knauer, P. Kornejew, B. Kursinski, H. Laqua, J. Meineke, H. T. Mora, and R. C. Wolf, Real-time dispersion interferometry for density feedback in fusion devices, J. Instrum. **13** (09), P09002.

[73] O. P. Ford, L. Vanó, J. A. Alonso, J. Baldzuhn, M. N. A. Beurskens, C. Biedermann, S. A. Bozhenkov, G. Fuchert, B. Geiger, D. Hartmann, R. J. E. Jaspers, A. Kappatou, A. Langenberg, S. A. Lazerson, R. M. McDermott, P. McNeely, T. W. C. Neelis, N. A. Pablant, E. Pasch, N. Rust, *et al.*, Charge exchange recombination spectroscopy at Wendelstein 7-X, Rev. Sci. Instrum. **91**, 023507 (2020).

[74] A. Langenberg *et al.*, Prospects of X-ray imaging spectrometers for impurity transport: Recent results from the stellarator Wendelstein 7-X (invited), Rev. Sci. Instrum. **89**, 10G101 (2018).

[75] O. P. Ford, A. Langenberg, T. Romba, P. Poloskei, M. Zanini, S. Bannmann, T. Gonda, K. Ida, R. L. Cansino, N. Pablant, J. de la Riva Villen, C. Swee, M. Yoshinuma, A. Alonso, B. Geiger, V. Perseo, E. Viezzer, and W7-X Team, Visible core spectroscopy at Wendelstein 7-X, Rev. Sci. Instrum. **95**, 083526 (2024).

[76] M. Grahl, J. Svensson, A. Werner, T. Andreeva, S. Bozhenkov, M. Drevlak, J. Geiger, M. Krychowiak, and Y. Turkin, Web services for 3D MHD equilibrium data at Wendelstein 7-X, IEEE Trans. Plasma Sci. **46**, 1114 (2018).

[77] S. Hirshman, W. van RIJ, and P. Merkel, Three-dimensional free boundary calculations using a spectral Green's function method, Comput. Phys. Commun. **43**, 143 (1986).

[78] M. Wappl, S. A. Bozhenkov, T. Andreeva, S. Bannmann, H. M. Smith, R. C. Wolf, and the W7-X Team, Experimental power balance study on turbulent heat transport at Wendelstein 7-X, Plasma Phys. Controlled Fusion **67**, 075025 (2025).

[79] T. Andreeva, J. Geiger, A. Dinklage, G. Wurden, H. Thomsen, K. Rahbarnia, J. Schmitt, M. Hirsch, G. Fuchert, C. Nührenberg, A. Alonso, C. Beidler, M. Beurskens, S. Bozhenkov, R. Brakel, C. Brandt, V. Bykov, M. Grahl, O. Grulke, C. Killer, *et al.*, Magnetic configuration scans during divertor operation of Wendelstein 7-X, Nucl. Fusion **62**, 026032 (2022).

Correction: The name F. Warmer was missing from the author list at publication and has been inserted as the 20th author.